JACS
JOURNAL OF THE AMERICAN CHEMICAL SOCIETY
Article
pubs.acs.org/JACS

Twisted Mannitol Crystals Establish Homologous Growth Mechanisms for High-Polymer and Small-Molecule Ring-Banded Spherulites

Alexander G. Shtukenberg,* Xiaoyan Cui, John Freudenthal, Erica Gunn, Eric Camp, and Bart Kahr*

Department of Chemistry, New York University, 100 Washington Square East, New York, New York 10003, United States

ABSTRACT: D-Mannitol belongs to a large and growing family of crystals with helical morphologies (Yu, L. *J. Am. Chem. Soc.* **2003**, *125*, 6380). Two polymorphs of D-mannitol, α and δ, when grown in the presence of additives such as poly(vinylpyrrolidone) (PVP) or D-sorbitol, form ring-banded spherulites composed of handed helical fibrils, where the helix axes correspond to the radial growth directions. The two polymorphs form helices with opposite senses in the presence of PVP but the same sense in the presence of D-sorbitol. The characteristic dimensions of the fibrils, including thickness, aspect ratio, and pitch, were determined by scanning probe and electron microscopies. These values must form the basis of any theory that presupposes what forces give rise to crystal twisting, a problem that has been broached but unsettled in the literature of polymer crystallization. The interdependence of the rhythmic variations of both linear and circular birefringence, as determined by Mueller matrix microscopy, informs the cooperative organization of mannitol fibers. The microstructure of mannitol ring-banded spherulites compares favorably to that of high polymers and is evaluated within the context of current theories of crystal twisting.

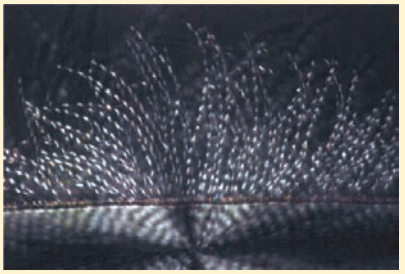

INTRODUCTION

The relationship between dissymmetric crystal forms (e.g., Pasteur's tartrate hemihedra) and molecular structure played a central role in the development of structural chemistry.[1] However, the mechanism of the expression of molecular dissymmetry in crystal morphology is often a mystery. In the last decade of the 19th century[2] and the first decade of the 20th,[3−16] when crystals with decidedly noncrystallographic helical morphologies were discovered, there was a determination to characterize these objects in order to build a bridge between microscopic and macroscopic chiral forms. In helices, crystalline dissymmetry was vividly illustrated.

A majority of twisted crystals appear as fibers composing ring-banded spherulites, radial aggregates with concentric optical rhythm arising from a precession of the optical indicatrix. Ring-banded spherulites are made from small organic compounds,[17−23] polymers,[24−29] and elements[30−32] grown from melts as well as from solution-grown minerals such as chalcedony.[33,34] Their fibrils are typically 5 nm to 3 μm thick with pitches between 500 nm and 1 mm. Twisted morphologies are also known for discrete crystals (thickness 1 μm to 10 cm) of various inorganic (potassium dichromate,[35−37] quartz,[38,39] mica,[38,40] gypsum[41−43]) and organic compounds (oxalic acid dihydrate,[38,44,45] hippuric acid,[46,47] decacyclene,[48] and a radical cation of 1,4-bis[2-(pyren-1-yl)vinyl]-2,5-dimethylbenzene[49]) as well as a protein (sickled hemoglobin).[50]

While some judgments have been drawn concerning the twisting mechanisms for large mineral single crystals (0.1 mm to 10 cm),[38,41] mimicking mineral growth in the laboratory is problematic. Twisting mechanisms have been studied in-depth for synthetic polymer spherulites only, because material properties take on added meaning for compounds industrially manufactured on a massive scale.[24] Polymer fibers (lamellae) are extremely fine (thickness 5−20 nm, width up to 1−3 μm). Their growth is complicated by noncrystalline polymer fractions, polydispersity, and phase transformations in the melt.

Comparatively little is known about the twisting mechanisms of molecular crystals.[30,31,46] Ring-banded spherulites are composed of fibers intermediate in thickness between molecularly thin polymer lamellae and large single crystals. As such, they reach to the extremes in both directions and may serve to articulate a comprehensive theory of crystal twisting phenomena. Therefore, this paper aims (1) to find an appropriate place for twisted molecular crystal spherulites within the kingdom of twisted crystals and (2) to establish how the twist intensity depends on the fiber thickness. This information is critical for an understanding of the twisting mechanism. D-Mannitol (Scheme 1) is a prototypical ring-banded spherulite.[51−53]

RESULTS

Crystal Optics. Mannitol crystallizes in three polymorphic modifications: α, β, and δ.[54] Only α and δ form from supercooled melts. The stable α modification melts at T_m = 166 °C and crystallizes in the orthorhombic $P2_12_12_1$ space group, whereas the metastable δ phase melts at 155 °C and forms monoclinic $P2_1$ crystals. Pure mannitol usually crystallizes as the α polymorph (sometimes δ as well) and forms nonbanded spherulites from 100 to 166 °C. Below this range, nucleation

Received: January 10, 2012
Published: March 13, 2012

   dx.doi.org/10.1021/ja300257m | *J. Am. Chem. Soc.* 2012, 134, 6354−6364

Scheme 1. D-Mannitol

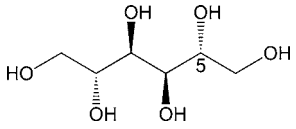

was too fast for crystallization to be observed. Spherulites of both polymorphs become optically banded (Figure 1) when mannitol is crystallized in the presence of an additive such as poly(vinylpyrrolidone) (PVP) (as discovered by Yu[51]) or D-sorbitol, a stereoisomer of mannitol differing only in the configuration at C5 (Scheme 1). The helical twisting of mannitol fibers was confirmed by "sensing the screw":[55−58] when a crystal was tilted around its elongated axis, interference colors observed between crossed polarizers were shifted up or down along the fiber depending on the helix sense. δ fibers are right-handed when they crystallize in the presence of PVP or sorbitol. α fibers are left-handed when they crystallize in the presence of PVP and right-handed when they crystallize in the presence of sorbitol.

As the temperature decreases below T_m, the growth rate first increases and then decreases, forming a broad maximum typical for melt-grown crystals (Figure 2a). The growth rate also decreases as the additive concentration increases (Figure 2b). The growth kinetics of pure α and δ mannitol is provided in ref 59.

An admixture of 15 wt % PVP favors crystallization of δ from 100 to 155 °C. α and δ coexist between 90 and 115 °C. At lower temperatures, only α grows. A sorbitol admixture (15 wt %) gives predominantly α from 75 to 166 °C; δ appears in small amounts between 75 and 110 °C. The twist period or pitch, P, (π rotation of the fiber around its axis; twist angle $\theta = \pi/P$) decreases sharply for both polymorphs as the growth temperature decreases (Figure 3a). For α with a PVP concentration (c_{PVP}) of 5 wt %, however, the effect of growth temperature is not monotonic (Figure 3b). As the temperature decreases, the twist period first decreases and then increases, with eventual formation of untwisted fibers from 80 to 115 °C. At lower temperatures the pitch decreases again. The effect of impurity concentration was measured only for the PVP additive (Figure 3c,d), which typically induces stronger twisting in both polymorphs. Sorbitol apparently does not induce twisting up to $c_{sorbitol}$ = 10 wt %; at 10−25 wt %, the pitch progressively decreases.

δ spherulites direct the refractive index n_Z radially, and the birefringence oscillates from $n_Z - n_Y = 0.015$ (dark rings) to $n_Z - n_X = 0.024$ (bright rings) (Figure 1a−c). These values are larger than what was reported previously.[60] According to X-ray diffraction from the sample surface, the [010] axis is perpendicular to the substrate (i.e., $n_Y \parallel$ [010]) in bright rings, and the [001] axis is close to the fiber elongation direction.

α spherulites direct n_Y radially, so the birefringence varies from the biggest value ($n_Y - n_X = 0.007$) in broader bands, passes through zero (the optic axis outcrop), and peaks at $n_Z - n_Y = 0.004$ in thinner bands. The optic axis angle was calculated from distances between optic axes outcrops ($2V = 69°$). In this

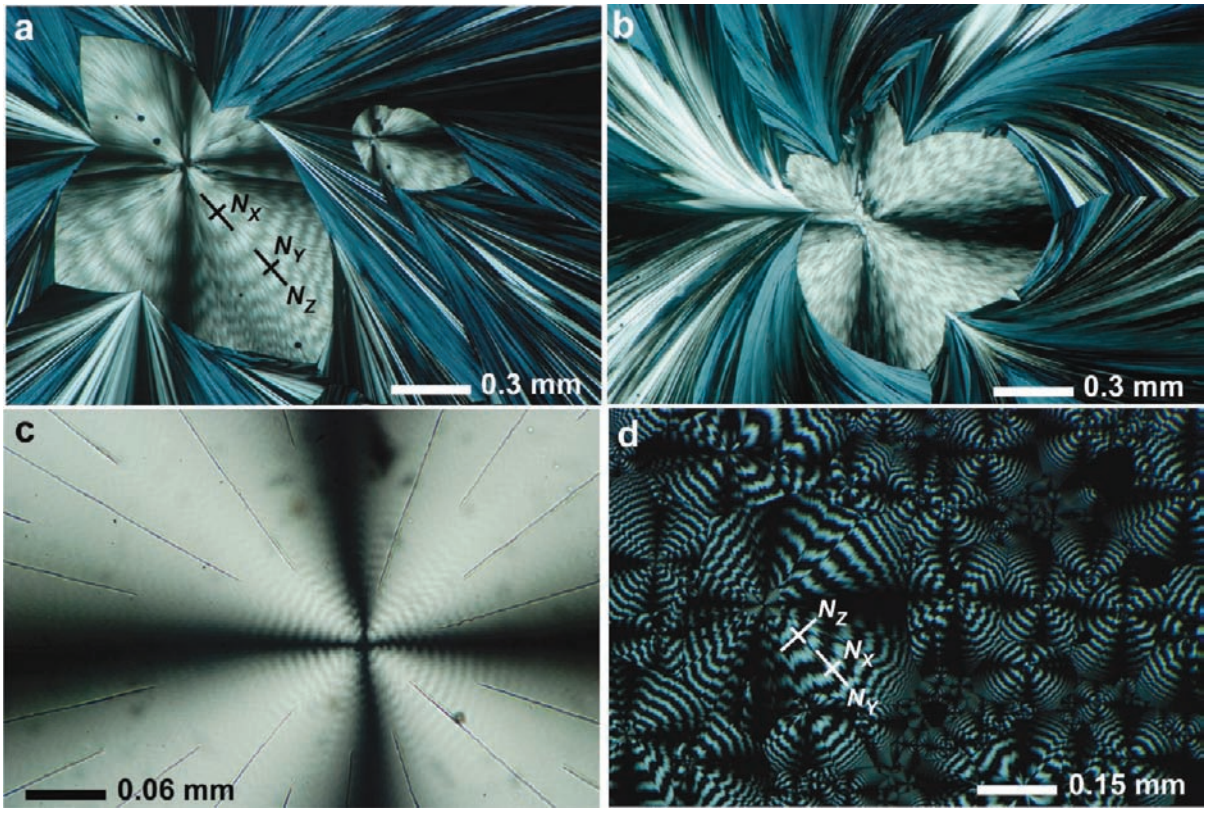

Figure 1. Mannitol spherulites viewed between crossed polarizers. (a, b) Spherulites of δ surrounded by unbanded α: (a) c_{PVP} = 5 wt %, T = 105 °C; (b) $c_{sorbitol}$ = 15 wt %, T = 105 °C. (c) Spherulite of δ. The banding fades with the distance from the center; c_{PVP} = 15 wt %, T = 100 °C. (d) Spherulites of α with very small areas of δ in their cores; c_{PVP} = 5 wt %, T = 60−80 °C. The orientation of the principal refractive indices is indicated for each polymorph. The absolute lengths of the crossed-index indicators are not meaningful. Typical films were between 3 and 4 μm in thickness.

dx.doi.org/10.1021/ja300257m | J. Am. Chem. Soc. 2012, 134, 6354−6364

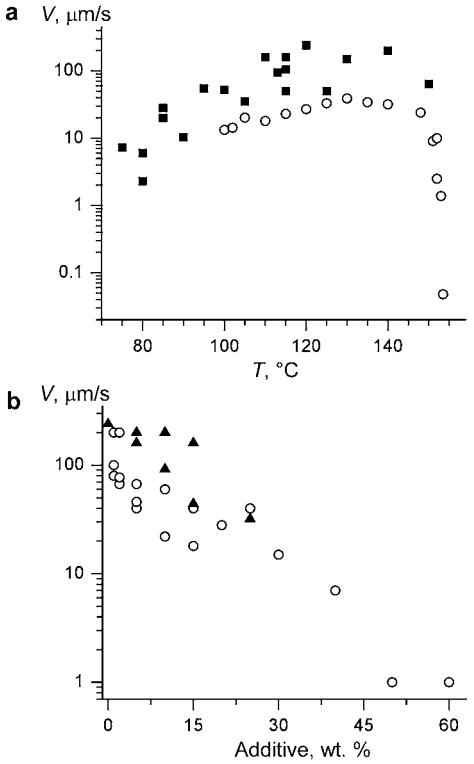

Figure 2. (a) Growth rate of mannitol as a function of growth temperature: circles, δ (c_{PVP} = 15 wt %); squares, α ($c_{sorbitol}$ = 15 wt %). (b) Growth rate as a function of additive concentration at T = 110 °C: circles, δ admixed with PVP; triangles, α admixed with sorbitol.

case, the measured optical properties are consistent with those previously reported: n_X = 1.526, n_Y = 1.536, n_Z = 1.540, (−)2V = 60° and n_X = 1.532, n_Y = 1.545 (calc.), n_Z = 1.550, (−)2V = 60°, n_X ∥ [010], n_Y ∥ [100], n_Z ∥ [001].[60,61]

Banded spherulites of α and δ were further analyzed by Mueller matrix imaging polarimetry. Mueller matrix imaging polarimetry which analyzes the polarization properties of a sample in terms of the transformation of an input Stokes vector ($\mathbf{S}_{in}$) via the 4 × 4 Mueller matrix **M**: $\mathbf{S}_{out} = \mathbf{M}\mathbf{S}_{in}$.[62] A Mueller matrix microscope (MMM) is a crossed-polarizer microscope with two rotating quarter-wave plates added above and below the sample that act as a complete polarization state generator (PSG)/polarization state analyzer (PSA) pair. When images are collected as a function of rotations of the PSA and PSG, the recorded intensities can be used to evaluate **M** for a sample at each pixel through pseudoinversion.[63] An MMM generates 16 images, each representing one element of **M** expressed in terms of measurable input and output polarization state intensities. Our instrument is based on designs found elsewhere.[64−66]

The 16 images are not simply related to the fundamental optical constants of interest: absorbance (A), linear birefringence (LB = $2\pi\Delta nL/\lambda$, where L is the thickness, λ is the wavelength, and Δn is the refractive index difference for orthogonal polarizations), linear birefringence with axes at 45° with respect to those of LB (LB′), linear dichroism (LD), linear dichroism with axes at 45° with respect to those of LD (LD′), circular birefringence [CB = $2\pi(n_L - n_R)L/\lambda$, where n_L and n_R are the refractive indices for left and right circularly polarized light], and circular dichroism (CD).[67]

To achieve the separation of optical effects, we implemented the analysis of Arteaga and Canillas.[68] Images corresponding to the matrix elements LB and CB are given in Figures 4 and 5. Since the crystal twists around the growth direction, the LB oscillates along the spherulite radii (Figures 4c and 5c) with the period P equal to π rotation of the crystallite. Two types of maxima with different LB values exist in the case of α (Figure 4a) because only absolute values of LB can be found from the analysis of MMM images. Thus, instead of a smooth sine like curve going through zero twice in one period. For both forms, the CB alternates between positive and negative values (Figures 4c and 5c). CB oscillations could in principle be a consequence of the anisotropy of the natural optical activity of mannitol polymorphs. However, optical rotation due to the crystal structure of mannitol, albeit β-mannitol only, is monosignate with values reaching −56 deg/mm, which is ca. 20 times smaller than that observed for the spherulites here.[69] The sinusoidal oscillations of CB and LB have the same period, P. However, generally speaking, |CB| is a minimum where LB is a maximum (Figures 4c and 5c).

Near the melting point (T > 145 °C), isolated needles and open spherulites predominate. The morphology of the individual needles is clear for δ grown in the presence of PVP (Figure 6). The width varies along the growth direction as a result of helical twisting of needles, with alternating flat-on (blue arrows in Figure 6) and edge-on (red arrows in Figure 6) orientations that correspond to LB maxima and minima, respectively. Isolated, twisted mannitol fibers actually untwist as they grow and thicken. This process resembles the untwisting of single fibers of hippuric acid grown near the melting point.[46] Unfortunately, the smaller LB of mannitol made it difficult to measure the untwisting dynamics.

Microstructural Analysis. At lower temperatures, mannitol forms compact spherulites with much finer fibers whose morphology was observed with atomic force microscopy (AFM) and scanning electron microscopy (SEM). α crystallites are lamellar (Figures 7 and 8b) with thickness (h):width (H) ratios ranging from 1:2 to 1:4 (absolute values: h = 0.13−0.33 μm and H = 0.5−1 μm). Poor-quality surfaces restricted observations to T = 85−100 and 80−110 °C for PVP and sorbitol admixtures, respectively. Within these ranges, h and H vary significantly for both admixtures and do not show a clear temperature dependence.

δ crystallites are also lamellar (Figures 8 and 9) with h:H typically ranging from 1:4 to 1:12. In comparison with PVP, sorbitol leads to thicker, wider lamellae (Figure 5a,b) [h = 0.03−0.4 μm and most often 0.05−0.25 μm; H = 0.15 − 2 μm (Figure 10)].

A dramatic demonstration of the helical twisting of mannitol spherulite fibrils is in evidence at the boundary between a ring-banded δ spherulite growing from the melt and a vaporous bubble (Figure 11). When the mannitol fibers grow into the bubble, either through diffusion along fibrils[70] or by sublimation, they become starved for nutrient. Close-packed spherulites become open with individual fibrils leaping into the void like coils released from an old mattress.

DISCUSSION

Mannitol among Other Twisted Crystals. To the best of our knowledge, the microstructure of an organic molecular spherulite has never been as fully characterized as that of mannitol described herein. Like high polymers,[24,25,29,55,71,72] mannitol twists as thin ribbons. Polymer spherulites are typically characterized by lamellae with thicknesses of 5−15 nm and widths of 0.2−3 μm (aspect ratio of 20−200),[29] whereas mannitol lamellae are 30−400 nm thick and 0.15−2

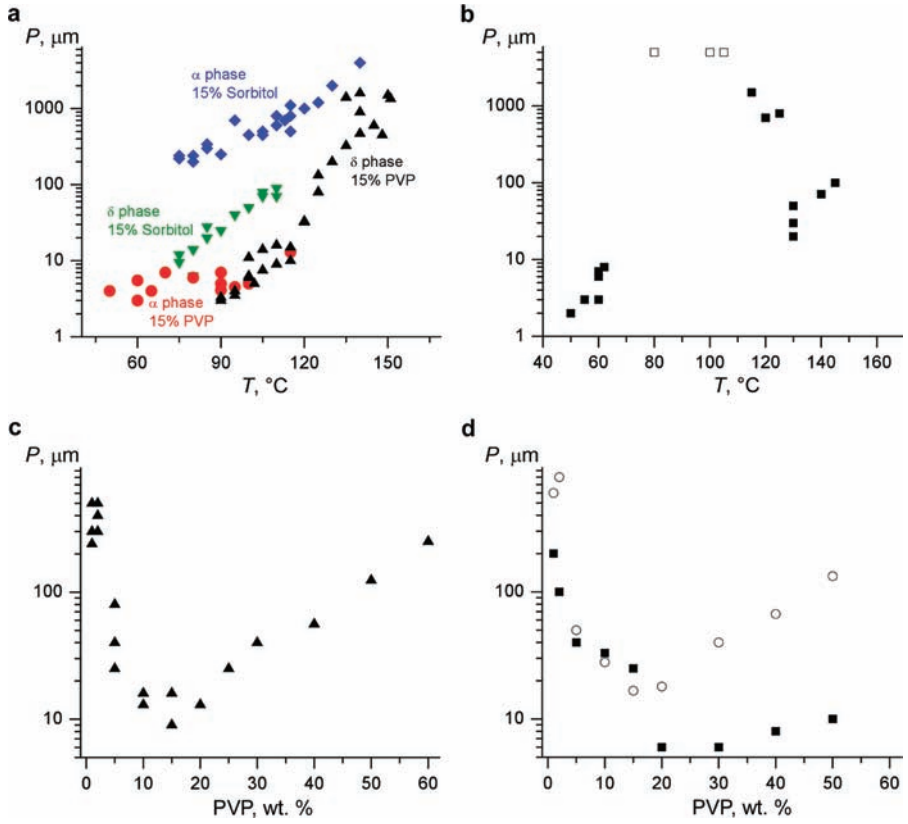

Figure 3. (a, b) Effect of growth temperature, T, on the twist period, P. Up and down triangles = δ; circles, squares, and diamonds = α. Up triangles and circles, c_{PVP} = 15 wt %; squares, c_{PVP} = 5 wt % (open squares show that fibers are untwisted or twisted with P > 5 mm); down triangles and diamonds, $c_{sorbitol}$ = 15 wt %. (c, d) Effect of PVP concentration on the twist period of δ. Triangles, T = 110 °C; squares, T = 100 °C; circles, T = 115 °C.

μm wide (aspect ratio of ca. 10). The thinnest mannitol lamellae grown at T < 100 °C (Figure 10a) are comparable to polymer lamellae of above-average thickness. The aspect ratios are large in both cases. Tightly packed planks cannot twist independently of one another. For both mannitol and high polymers, geometrical constraints force bunching and cooperativity (cf. Figure 9a,b and Figures 5 and 6 in ref 29; also see refs 24 and 71−74).

The arrangement of twisted lamellae in a spherulite can be clearly seen for δ grown in the presence of PVP. In the edge-on orientation, the lamellae are parallel to each other (Figure 9a) and projections of their optical indicatrices lie in the plane perpendicular to the light's wave vector. As lamellae twist and deviate from the edge-on orientation, they start to compete for space. AFM images show that lamellae form bunches (10−15 lamellae/bunch) where they change their orientations not simultaneously but in a sequence (Figure 9a). They stick to one another, mutually impeding growth. Sometimes they change orientation slightly, thereby avoiding collisions by splaying. Here, the LB takes on intermediate values between edge-on maxima and flat-on minima (Figures 4c and 5c).The splaying is characterized by progressive angular misorientations that result in CB of one sign.

CB resulting from splaying of anisotropic lamellae is consistent with the very first model of optical activity, Reusch's pile of twisted mica plates.[75,76] Reusch recognized that he could mimic optical rotation in crystals by stacking flakes of mica each rotated in the same sense by a small amount from layer to layer. We applied the idea of misoriented anisotropic lamellae to explain the CB of poly(lactic)acid.[77]

Continued twisting results in flat-on orientations, in which the lamellae lie in a common plane or planes parallel to the substrate. Here the LB reaches its maximum value (Figure 9a) while the CB remains close to zero. This occurs for the following reasons: (1) The thickness of a single layer is much smaller than the thickness of a mannitol film (3−4 μm), and this space is occupied by several bunches of lamellae or several tens of individual lamellae (Figure 9a). Misorientations between bunches can cancel the CB generated by lamellae in individual bunches. (2) Misorientations in flat-on regions are reduced since only lamellae with the highest radial growth rates can survive during rotation from edge-on to flat-on orientations. Crystallites whose fastest growth direction significantly deviates from the radial orientation stick to other crystallites and stop growing. The absence of CB in flat-on regions tells us that misorientations are either absent or chaotic.

The return from the flat-on to the edge-on orientation resembles the edge-on to flat-on transition but with the opposite splay sign and corresponding oppositely signed CB. The individual fibrils show LB but no evidence of CB. This is further evidence that CB results from the *cooperation* of lamellae.

The complex, cooperative character of twisting results in the eventual loss of coherence in lamellae orientations. Optical bands often become fuzzy as the distance from the spherulite center increases (Figure 1c). The loss of coherence can be also observed in AFM images.

The smooth transition between individual twisted crystals and spherulite fibers in both hippuric acid[17] and mannitol appears to indicate a common mechanism of growth. As the

dx.doi.org/10.1021/ja300257m | J. Am. Chem. Soc. 2012, 134, 6354−6364

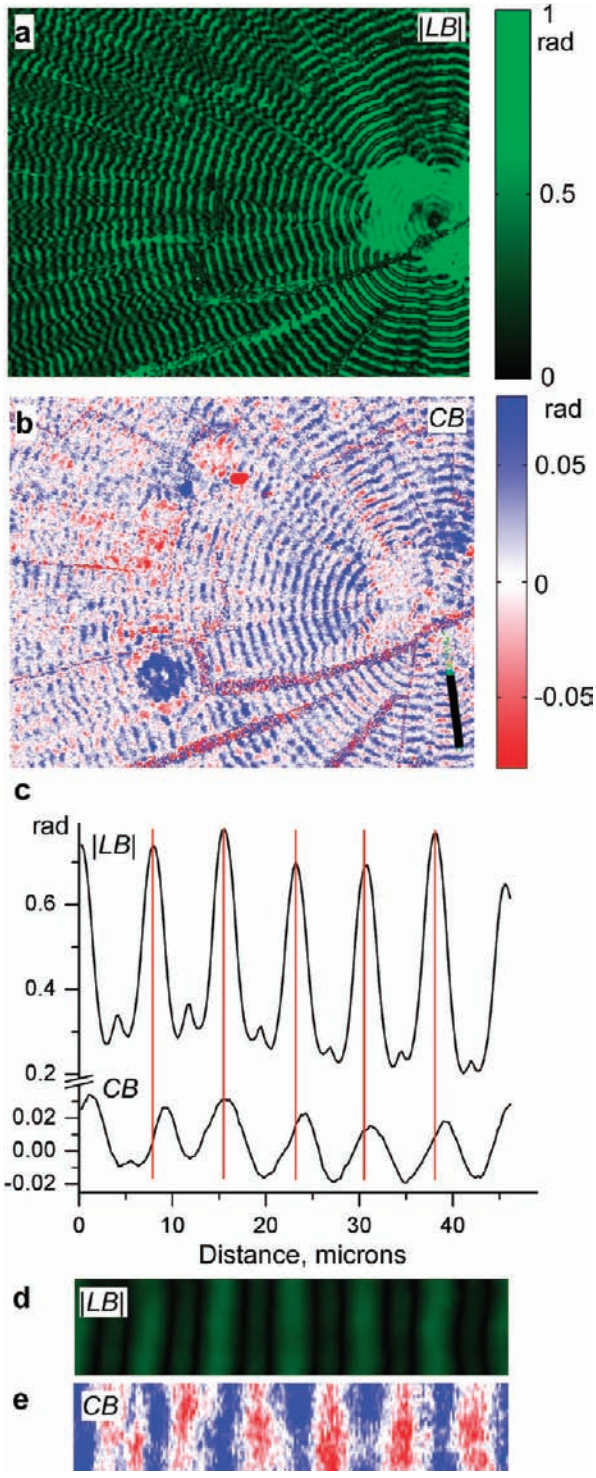

Figure 4. (a, b) MMM images of α with c_{PVP} = 15 wt % at T = 95 °C: (a) linear retardance (conventionally indicated as LB in Mueller matrix microscopy); (b) circular retardance (conventionally indicated as CB in Mueller matrix microscopy). (c) Plot drawn along the path indicted by the black line in (b). The optical properties in the plot were averaged over four lateral pixels (1.05 μm). Vertical red lines highlight shifts between the LB and CB extrema. The LB is usually largest when the CB is small, except at 15 μm, where there is an anomaly. (d, e) Enlarged parts of (a) and (b) drawn along the same line as the plot in (c).

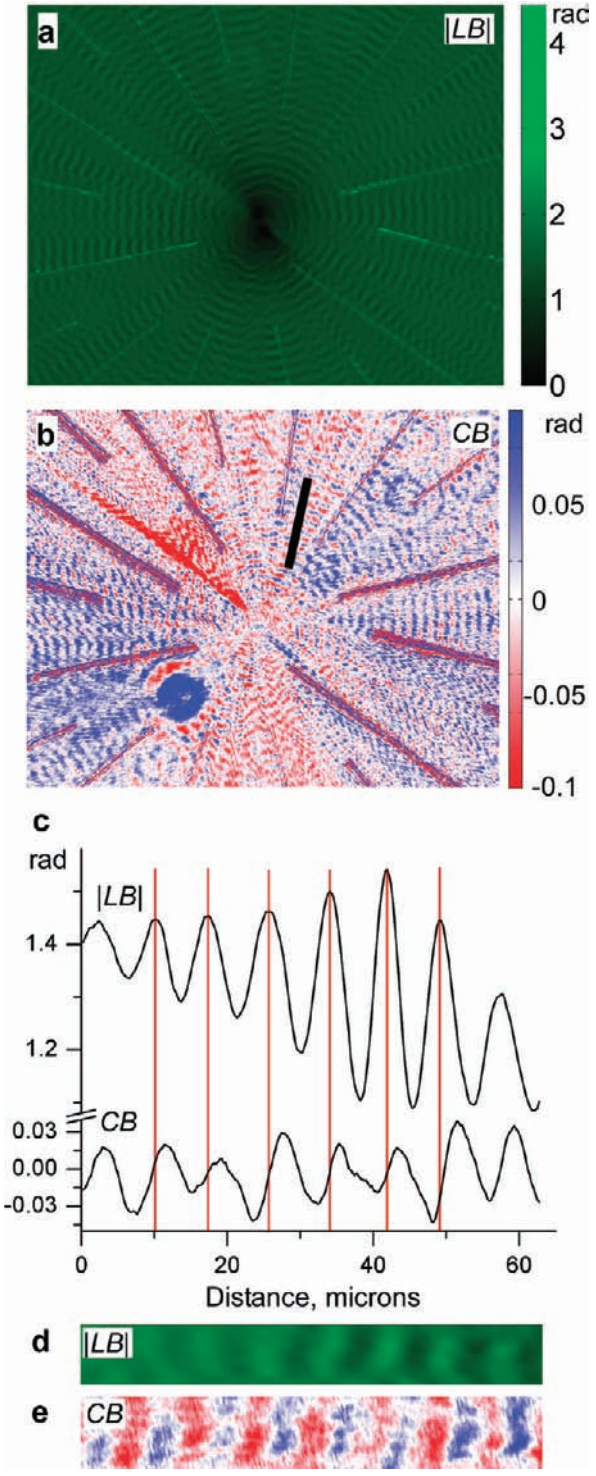

Figure 5. (a, b) MMM images of δ with c_{PVP} = 15 wt % at T = 110 °C: (a) linear retardance (conventionally indicated as LB in Mueller matrix microscopy); (b) circular retardance (conventionally indicated as CB in Mueller matrix microscopy). (c) Plot drawn along the path indicted by the black line in (b). Optical properties in the plot were averaged over four lateral pixels (1.05 μm). Vertical red lines highlight shifts between the LB and CB extrema. (d, e) Enlarged parts of (a) and (b) drawn along the same line as the plot in (c).

mannitol crystallization temperature drops, the twist period P gradually decreases, as has been observed for most polymers.[26−29,78−80] At the same time, individual fibers are replaced with compact spherulites, accompanied by decreasing fiber thickness (from 3 to 0.3 μm) and width (from 20−30 to 1.5 μm) as shown in Figure 10a. This dramatic change reflects

dx.doi.org/10.1021/ja300257m | J. Am. Chem. Soc. 2012, 134, 6354−6364

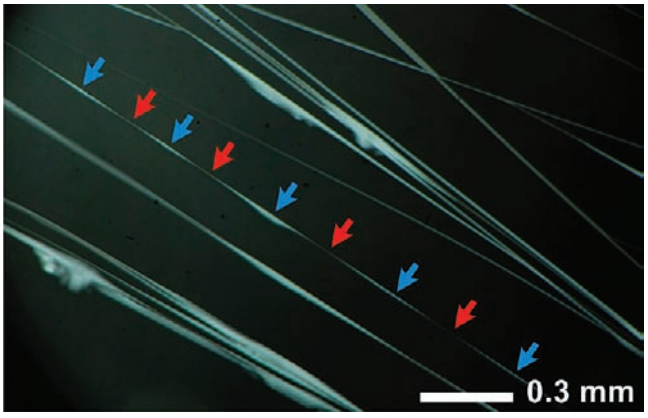

Figure 6. Isolated needles of δ growing from the melt at ca. 150 °C with c_{PVP} = 10 wt %. Periodic variations of thickness and transmitted intensity are associated with helical twisting of the fibers. Edge-on and flat-on orientations are indicated by red and blue arrows, respectively.

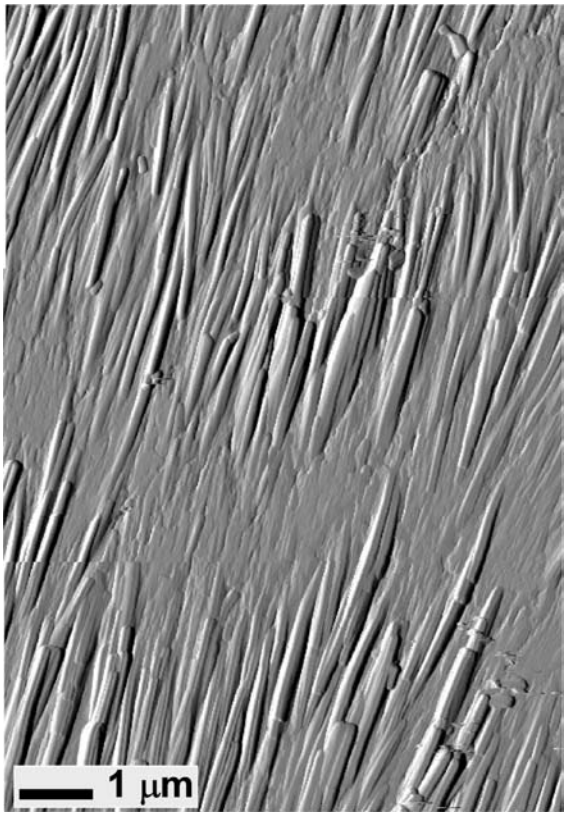

Figure 7. AFM deflection images of α spherulite (c_{PVP} = 15 wt %, T = 95 °C, P = 6 μm).

the fact that isolated fibers can freely grow in all directions and have enough time to acquire significant size, whereas lamellae in spherulites are tightly packed and their thickness is primarily dictated by geometrical selection.[81]

Twisting Mechanisms. The literature has promulgated as many as four main mechanisms of crystal twisting. Three have competed for the attention of polymer scientists and are summarized by Lotz and Cheng;[24] a fourth mechanism has primarily been applied to bulk crystals.[38] These are briefly outlined below.

1. Axial *screw dislocations* in thin rods (Eshelby twisting)[82] or isochiral transverse screw dislocations in lathlike crystals drive twisting from within.[83,84] Such dislocations form a stress field that induces a twist moment in the crystallite. Although this mechanism was found to operate in some special cases such as PbS[85] and PbSe[86] nanowires, its applicability should be restricted. For lathlike polymer lamellae, twisting was shown to be independent of the presence of transverse screw dislocations.[24] For rodlike single crystals, Eshelby's mechanism predicts twist periods that are too large.[38,46] Moreover, banded spherulites composed of twisted fibers are remarkably homogeneous. The necessity of the same dislocation structure for all fibers seems unlikely given the stochastic character of dislocation formation.
2. *Fields* that form around growing crystals, including thermal (from the latent heat of crystallization), concentration (from the exclusion in the melt of impurities by the growing crystal), and/or mechanical (from density variation between crystal and melt) fields, force reorientation during growth.[27−29,87] The applicability of this mechanism seems to be questionable for the following reasons: (1) Spherulites of the same compound formed under similar growth conditions can show different degrees of twisting.[17,46] (2) For the same compound under the same conditions, both single crystals and spherulites can have similar twist periods. Moreover, spherulites formed under different mass and heat transport conditions can likewise show similar twist periods.[17,24,46] (3) The twist intensity can be very sensitive to minor impurities.[88] This is also true for mannitol, which can form crystals with the same pitch either as fibers in spherulites or as individual crystals

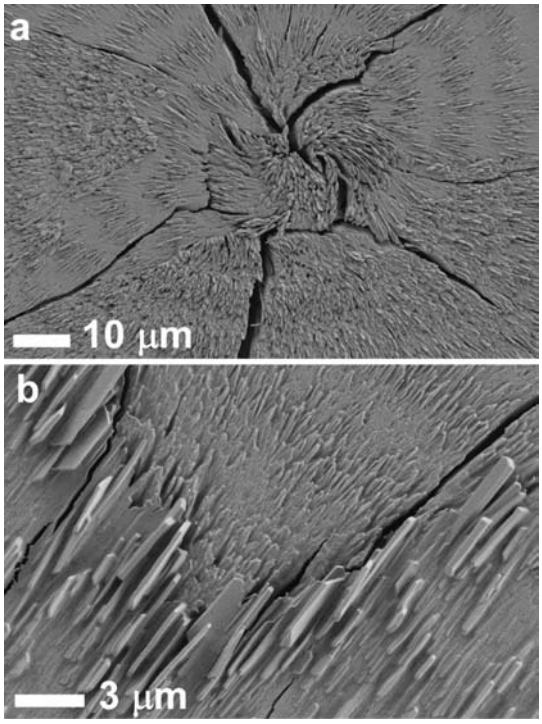

Figure 8. SEM images of mannitol spherulites grown in the presence of 15 wt % PVP. (a) δ mannitol, T = 110 °C, P = 30 μm, T = 105 °C. (b) Cross-nucleation of α (P = 5 μm) on the growth front of δ (P = 7.5 μm). Well-shaped, edge-on δ plates were probably formed during postgrowth mannitol recrystallization, when the coverslip was removed.

dx.doi.org/10.1021/ja300257m | J. Am. Chem. Soc. 2012, 134, 6354−6364

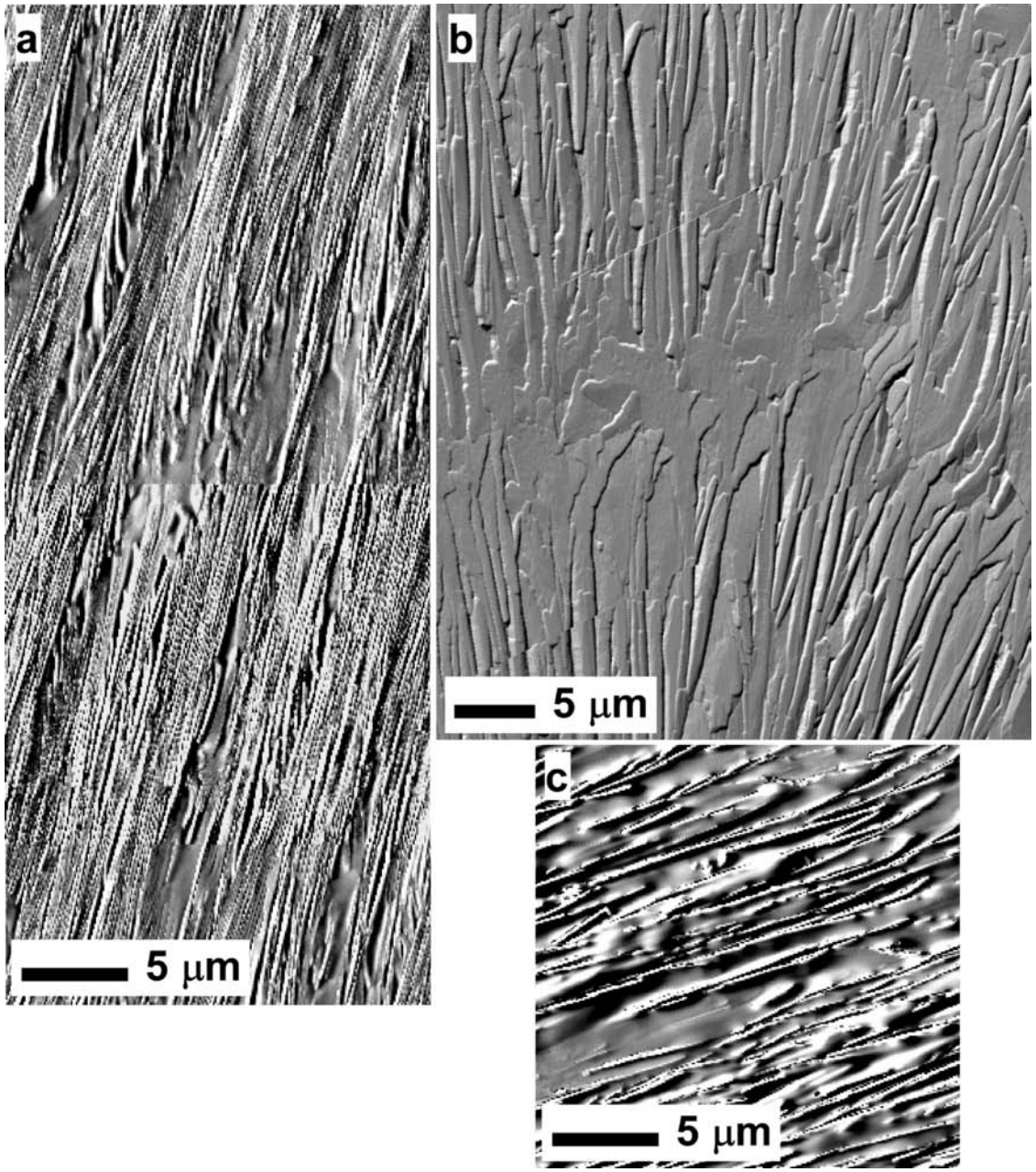

Figure 9. AFM deflection images of δ spherulites. (a) c_{PVP} = 15 wt %, T = 120 °C, P = 33 μm. (b) $c_{sorbitol}$ = 15 wt %, T = 90 °C, P = 40 μm. (c) c_{PVP} = 40 wt %, T = 110 °C, P = 56 μm.

(Figure 10a) and whose twist period is highly sensitive to additives.

3. Anisotropic *surface stresses* due to structural differences between a surface layer and the bulk deform the crystal.[24,25,89,90] This hypothesis can work only if the thickness of the surface layer (typical thickness of 1 nm) is comparable with the thickness of the whole crystal. It is quite possible for polymer lamellae with a total thickness of 5−20 nm but unlikely for thicker objects such as mannitol lamellae (>30 nm) as well as individual fibers that are several micrometers thick.
4. *Autodeformation* results from the difference in structure and growth rates of symmetry-independent facets or vicinal facets in the presence of impurities. It can lead to differences in lattice constants in adjacent growth sectors and ultimately to misfit (heterometry) stress and strain.[91] For some crystal morphologies, this stress can create a macroscopic twist moment. The resulting twist may be preserved in the crystal volume in the course of plastic stress relaxation.[38,41,46] The applicability of this mechanism was well-illustrated for single crystals of quartz[38] and oxalic acid dihydrate[38,44] and, to a lesser extent, for single crystals of gypsum,[41] mica,[38,40] and hippuric acid.[46] The autodeformation hypothesis is capable of explaining fiber twisting in spherulites of various substances, but it lacks direct evidence.

In summary, fields are probably not a source of crystal twisting, and while dislocations definitely occur in twisted crystals, they likely result from twisting forces and are not the source of the forces themselves. The two remaining mechanisms can be combined together, as the internal stresses

dx.doi.org/10.1021/ja300257m | J. Am. Chem. Soc. 2012, 134, 6354−6364

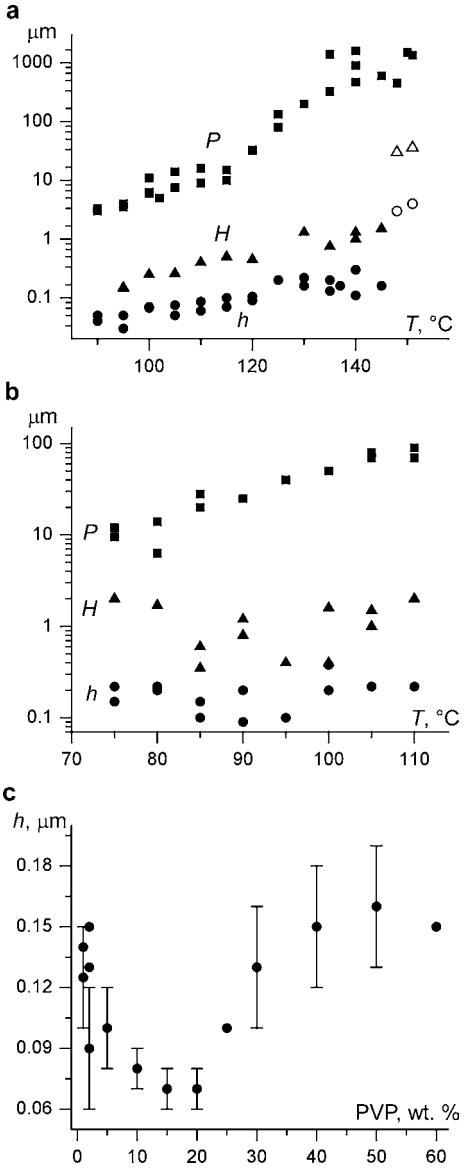

Figure 10. Effect of (a, b) the growth temperature and (c) the PVP concentration on the thickness h (circles) and width H (triangles) of mannitol lamellae: (a) c_{PVP} = 15 wt %; (b) $c_{sorbitol}$ = 15 wt %; (c) T = 110 °C. In (a) and (b), the twist period P (squares) is also indicated for comparison. Open symbols in (a) correspond to individual fibers and open spherulites, whereas solid symbols correspond to compact spherulites.

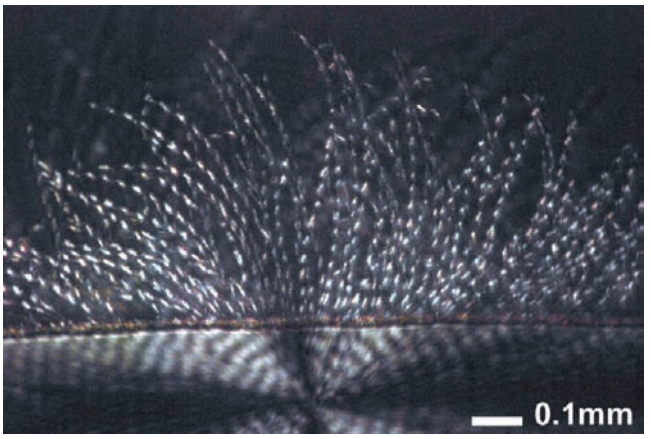

Figure 11. A compact banded mannitol spherulite growing from the melt (δ, T = 140 °C, c_{PVP} = 30 wt %) turns into an open spherulite with isolated twisted fibers when it penetrates into a vapor bubble.

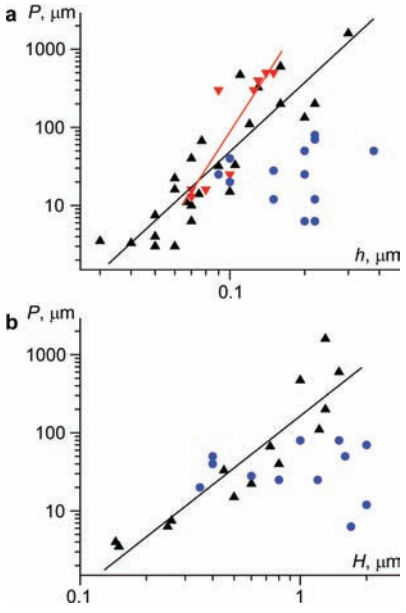

Figure 12. Effect of (a) the thickness h and (b) the width H on the twist period P of δ mannitol lamellae. Up triangles (black), c_{PVP} = 15 wt %, T = 90–145 °C; down triangles (red), T = 110 °C, PVP concentration varies; circles (blue), $c_{sorbitol}$ = 15 wt %, T = 75–110 °C. Lines are fit to a power function.

caused by inhomogeneity relax via macroscopic crystal deformation. In fact, surface stress is a specific kind of heterometry that becomes important for very thin objects.

Relation of Pitch and Fiber Size. The effect of lamellae thickness and width on the twist period (Figure 12) were evaluated by combining the data for $P(T)$ (Figure 3a) with those for $H(T)$ and $h(T)$ (Figure 10). For variable temperature and constant PVP concentration, $P \sim h^{2.9(3)}$ and $P \sim H^{2.2(3)}$. The pitch apparently changes sharply as the fibers narrow. On the other hand, for variable temperature and constant sorbitol concentration, the twist period seems to be independent of cross section. Such different behavior can be explained either via different twisting mechanisms for different additives or by assuming substantial independence of the twist intensity on the fiber thickness. The first possibility is unlikely since the optical patterns (Figure 1a,b), and morphology of the lamellae (Figure 9a,b), and $P(T)$ (Figure 3a) are very similar for mannitol spherulites grown in the presence of PVP and sorbitol additives.

Both P and h may be correlated with T, but this does not imply a causal relationship. In fact, thin lamellae in spherulites and isolated needlelike crystals grown in the presence of PVP at 140–151 °C are characterized by similar twist periods but have very different cross sections (Figure 10a).

While the dependences of P and h on the PVP concentration (Figures 3c,d and 10c, respectively) are similar, the logarithmic correlation (Figure 12a) is not tight [$P \sim h^{4.9(1.0)}$]. The lamellae thickness decreases rapidly with the introduction of PVP, probably because of impurity-intensified branching. However, at c_{PVP} = 2 wt %, the thinning process slows, whereas the rapid decrease in the twist period is extended up to $c_{PVP} \approx$ 10 wt %. The increased twist intensity can be explained through the direct action of the PVP additive. At c_{PVP} > 20 wt %, the

dx.doi.org/10.1021/ja300257m | J. Am. Chem. Soc. 2012, 134, 6354–6364

lamellae are not tightly packed and have more space for growth (Figure 9c), resulting in their thickening. On the other hand, the pitch increases as well via untwisting, as observed in situ for isolated mannitol fibers. In contrast, untwisting under crowded conditions is geometrically constrained, maintaining a smaller pitch. Moreover, at high mannitol concentration, the melting point progressively decreases (by ~10 °C at c_{PVP} = 60 wt %).[92] This diminishes the actual supercooling and should increase the twist period (at T = 110 °C, increasing T by 10 °C increases P from 12 to 33 μm; Figure 3a). This can explain the correlation of P and h over the whole range of PVP concentrations.

In spherulite lamellae, the thickness and width do not directly affect the twist period. This can be seen in $P(h)$ relationships in the literature for different twisted crystals (Figure 13). The exponent in the power law, $P = \text{const}\cdot h^n$, is

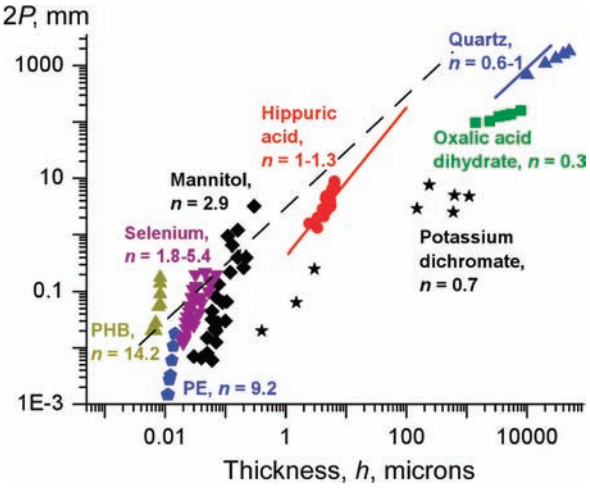

Figure 13. Correlation between full twist period ($2P$, 2π rotation, mm) and the smallest fiber size in a cross section (h, μm) for quartz single crystals (blue line[39] and blue up triangles[38]), oxalic acid dihydrate single crystals (olive squares),[38] potassium dichromate single crystals[35] and open spherulites[93] (black stars), δ mannitol spherulites with c_{PVP} = 15 wt % (black diamonds, present paper), hippuric acid single crystals (red circles[46] and red line[47]), two types of selenium spherulites (purple down triangles),[30,31] 32 kDa polyethylene (PE) spherulites (blue pentagons),[29] and poly[(*R*)-3-hydroxybutyrate] (PHB) spherulites (dark-yellow up triangles).[26] The values of n are exponents in the fit $P = \text{const}\cdot h^n$. In the region below the dashed line ($2P = 0.001\pi h$), the elastic stress in twisted crystals should relax in part.

very big (n = 9.2−14.2) for polymer spherulites but smaller for molecular crystal spherulites (n = 1.8−5.4), and it is close to n = 1 for single crystals. The big exponents for spherulites probably have no physical meaning; rather, they show that the $h(T)$ dependence is not strong, while the driving force for twisting is highly temperature-dependent and it primarily determines the twist period. For single crystals, the band spacing is known to be strongly controlled by fiber untwisting and roughly obeys the empirical expression $P = P_0 + P_1 h$ (P_0 and P_1 are constants), which leads to $n \approx 1$.[38,44,46]

In theory, the thicker the fiber, the weaker the twist intensity, because increased fiber rigidity should work against the twist moment applied to the crystal from internal or external forces. For a circular rod of radius r twisted by a torque or a twist moment, M, the twist period (π rotation) is expressed as $P = \pi/\theta = \pi GJ/M$, where G is the shear modulus and $J = \pi r^4/2$ is the torsion constant.[94] It follows that the torsion constant is proportional to the ratio of the torque to the twist angle, all else being equal. If it is assumed that the torque is homogeneously distributed over the side surface of the rod, which means that $M = 2\pi L r^2 \tau$, where L is the length of the rod and τ is the local stress on the surface responsible for the twist moment, then $P = \pi G r^2/(4\tau L)$. This expression changes only by a small constant factor for rods with noncircular cross sections and for twisting stresses distributed in the cross section along lines whose lengths are proportional to the radius (thickness) r. Such corrections should accommodate almost any type of internal or external stress and result in the general law $P \sim r^2/L$. However, this law has not been observed for fibers in spherulites or for single crystals (Figure 13).

There are two explanations for this failure: (1) the effects of temperature and other growth conditions are so strong that the effect of crystal thickness is not pronounced, and (2) stress forming at the crystal tip during growth immediately relaxes plastically. The first reason should be important for spherulites grown from the melt, for which even a small change in temperature can significantly affect the properties of the material and the crystallization processes. This argument does not apply to solution-grown crystals formed under near-constant effective growth conditions. The second reason should apply to all crystals. If elastic stress at the crystal tip is immediately released by plastic deformation, the crystal thickness and length cannot affect the twist period, and the crystal does not "feel" geometric dimensions. We have observed that individual twisted crystals of quartz, mica, hippuric acid, and oxalic acid dihydrate preserve their deformation state despite fragmentation, which would redistribute elastic deformation in the absence of plastic deformation. Polymer fibers can be isolated from spherulites by etching without a change in twist intensity.[24] The presence of plastic deformations has been shown for crystallites in banded selenium spherulites.[30] We have emphasized the plastic nature of twisting for single crystals of hippuric acid.[46] Here, we can extend this conclusion to mannitol.

The predominance of plastic deformations can be demonstrated by comparing the maximum elastic stress in a twisted crystal, $\tau_{max} = \theta r G = 2\pi r G/P$,[94] with the minimum stress needed for brittle or ductile deformation of crystals, $\tau_c = 10^{-3}G$.[95] Hence, the greatest twist possible within the elastic limit follows the relationship $2P = 0.002\pi r = 0.001\pi h$, which is shown as a dashed line in Figure 13. One can see that the data for most crystals, including polymers, lie below this line, indicating stress relaxation. Although in perfect nano-objects much larger elastic stress can exist and crystals can sometimes attain the theoretical strength $\tau_c = 0.1G$,[95] most banded spherulites grow from the melt, where the plasticity is usually high.

■ CONCLUSIONS

Ring-banded polymer spherulites have been studied intensively in the second half of the 20th century and beyond. Ring-banded small-molecule organic spherulites were studied intensively only in the first half of the 20th century and suffer by comparison, given the comparatively primitive methods of analysis available before 1950. While it is easy to imagine the accommodation of twisting by crystals composed of long-chain molecules, it is harder to reckon twisting in the mind's eye for, say, brittle sugar crystals. We previously showed that rhythmic precipitates and helical twisting both contribute to concentric optical contrast in spherulites.[17] Is the twisting in high polymers

and small molecules that give nearly identical polarized light micrographs driven by similar processes? A detailed investigation of ring-banded mannitol spherulites was undertaken here to put small organic molecules and high polymers on an equal footing, if possible.

Mueller matrix microscopy, AFM, and SEM studies of α and δ D-mannitol grown from the melt have shown in combination that spherulites are composed of lamellar fibers with thicknesses of 0.03−0.4 μm. In the presence of PVP and sorbitol additives, mannitol lamellae become twisted around their elongation axis. The sizes and shapes and the mutual arrangement of lamellae in a spherulite turn out to be very similar to those in polymer spherulies with twisted lamellae. We observed the growth of single twisted mannitol fibers and tracked the transformation of isolated crystals into spherulites with twisted fibers. This shows that twisting phenomena in ring-banded spherulites of polymers and molecular crystals as well as single crystals share essential qualities.

Periodic oscillations of the CB in banded mannitol spherulites result from periodic variations in the degree of misorientation of overlapping lamellae. Flat-on and edge-on lengths are characterized by approximately zero CB because the extinction directions in the laminated fibers are aligned. Absolute maxima in CB correspond to regions between the flat-on and edge-on extremes, where the splaying in the extinction directions is largest.

In mannitol spherulites, as well as in most other spherulites with twisted fibers, the twist period decreases nonlinearly with decreasing temperature. The lamellae thickness/width may also decrease, but no strong causal relationship between lamellae thickness/width and twist period is expected, probably because of the plastic character of twist deformation.

EXPERIMENTAL SECTION

Crystal Growth. Several milligrams of D-mannitol (Sigma-Aldrich) mixed with an additive, either PVP (Sigma-Aldrich, 10 kDa, c_{PVP} = 1−60 wt %) or D-sorbitol (Sigma-Aldrich, $c_{sorbitol}$ = 1−25 wt %), was placed on a glass slide, covered by a coverslip, and melted with a hot plate. Typical films were 3−4 μm thick. The samples were placed in a microscope hot stage, remelted at $T \approx 168$ °C, and cooled to a desired growth temperature. Growth rates were measured with a polarized light microscope by the advancement of the growth front with time.

Mueller Matrix Microscopy. Optical properties were established with a home-built MMM, which was previously described.[46] The samples were measured at the wavelength λ = 532 nm.

Atomic Force Microscopy. Height and deflection images were recorded with an MFP-3D-SA system (Asylum Research). Measurements were performed in contact mode at a deflection of −2.0 V on samples without cover slides.

Scanning Electron Microscopy. The samples were mounted on conductive carbon tapes after removal of the top coverslip, adhered on aluminum holders, and then coated with 5 nm of gold. The images were recorded with a MERLIN field-emission scanning electron microscope (Carl Zeiss) using a standard Everhart−Thornley type detector at an acceleration voltage of 1−2 kV.

X-ray Diffraction. Polymorph identification and indexing was carried out using an X-ray Bruker AXS D8 DISCOVER GADDS microdiffractometer equipped with a VÅNTEC-2000 two-dimensional detector and a 0.5 mm MONOCAP collimator (Cu Kα radiation).

AUTHOR INFORMATION

Corresponding Author

shtukenberg@mail.ru; bart.kahr@nyu.edu

Notes

The authors declare no competing financial interest.

ACKNOWLEDGMENTS

B.K. thanks the NSF (CHE-0845526) for support of this research. The authors acknowledge Dr. Chunhua Hu (NYU Department of Chemistry X-ray Diffraction Facility) and the NSF Chemistry Research Instrumentation and Facilities Program (CHE-0840277) for the powder microdiffractometer. The scanning electron microscope was purchased with financial support from the MRI Program of the National Science Foundation under Award DMR-0923251. We thank Professor Michael D. Ward for the use of his atomic force microscopes.

REFERENCES

(1) Mauskopf, S. H. *Trans. Am. Phil. Soc., New Ser.* **1976**, *66*, 1−82.
(2) Michel-Levy, A.; Munier-Chalmas, C. P. E. *Bull. Soc. Fr. Mineral.* **1892**, *15*, 159−190.
(3) Wallerant, F. *C. R. Acad. Sci. (Paris)* **1906**, *143*, 553−557.
(4) Wallerant, F. *C. R. Acad. Sci. (Paris)* **1906**, *143*, 1169−1170.
(5) Wallerant, F. *Bull. Soc. Fr. Mineral.* **1907**, *30*, 43−60.
(6) Gaubert, P. *C. R. Acad. Sci. (Paris)* **1908**, *146*, 829−831.
(7) Gaubert, P. *Bull. Soc. Fr. Mineral.* **1911**, *32*, 422−437.
(8) Gaubert, P. *C. R. Acad. Sci. (Paris)* **1911**, *153*, 683−685.
(9) Gaubert, P. *Ann. Chim. Phys.* **1916**, *5*−*6*, 356−364.
(10) Gaubert, P. *Bull. Soc. Fr. Mineral.* **1918**, *41*, 198−224.
(11) Gaubert, P. *Bull. Soc. Fr. Mineral.* **1918**, *167*, 368−370.
(12) Gaubert, P. *Bull. Soc. Fr. Mineral.* **1922**, *175*, 973−975.
(13) Bernauer, F. *"Gedrillte" Kristalle*; Gebrüder Borntraeger: Berlin, 1929.
(14) Gaubert, P. *Bull. Soc. Fr. Mineral.* **1925**, *80*, 1853−1855.
(15) Gaubert, P. *Festschrift Victor Goldschmidt*; Carl Winters Universitätsbuchhandlung: Heidelberg, Germany, 1928; pp 98−107.
(16) Gaubert, P. *C. R. Acad. Sci. (Paris)* **1931**, *92*, 1576−1579.
(17) Shtukenberg, A.; Gunn, E. G.; Gazzano, M.; Freudenthal, J.; Camp, E.; Sours, R.; Rosseeva, E.; Kahr, B. *ChemPhysChem* **2011**, *12*, 1558−1571.
(18) Hutter, J. L.; Bechhoefer, J. *J. Cryst. Growth* **2000**, *217*, 332−343.
(19) Sadlik, B.; Talon, L.; Kawka, S.; Woods, R.; Bechhoefer, J. *Phys. Rev. E* **2005**, *71*, No. 061602.
(20) Degen, M. M.; Costanzino, N.; Bechhoefer, J. *J. Cryst. Growth.* **2000**, *209*, 953−962.
(21) Hutter, J. L.; Bechhoefer, J. *J. Cryst. Growth* **2000**, *217*, 332−343.
(22) Pisula, W.; Kastler, M.; Wasserfallen, D.; Pakula, T.; Müllen, K. *J. Am. Chem. Soc.* **2004**, *126*, 8074−8075.
(23) Lin, T.-F.; Ho., R.-M.; Sung, C.-H.; Hsu, C.-S. *Chem. Mater.* **2006**, *18*, 5510−5519.
(24) Lotz, B.; Cheng, S. Z. D. *Polymer* **2005**, *46*, 577−610.
(25) Ye, H.-M.; Wang, J.-S.; Tang, S.; Xu, J.; Feng, X.-Q.; Guo, B.-H.; Xie, X.-M.; Zhou, J.-J.; Li, L.; Wu, Q.; Chen, G.-Q. *Macromolecules* **2010**, *43*, 5762−5770.
(26) Barham, P. J.; Keller, A.; Otun, E. L.; Holmes, P. A. *J. Mater. Sci.* **1984**, *19*, 2781−2794.
(27) Toda, A.; Taguchi, K.; Hikosaka, M.; Kajioka, H. *Polym. J.* **2008**, *40*, 905−909.
(28) Toda, A.; Taguchi, K.; Kajioka, H. *Macromolecules* **2008**, *41*, 7505−7512.
(29) Toda, A.; Okamura, M.; Taguchi, K.; Hikosaka, M.; Kajioka, H. *Macromolecules* **2008**, *41*, 2484−2493.
(30) Ryschenkow, G.; Faivre, G. *J. Cryst. Growth* **1988**, *87*, 221−235.
(31) Bisault, J.; Ryschenkow, G.; Faivre, G. *J. Cryst. Growth* **1991**, *110*, 889−909.
(32) Kozlovskii, M. I. *Sov. Phys. Crystallogr.* **1965**, *10*, 101−103.
(33) Frondel, C. *Am. Mineral.* **1978**, *63*, 17−27.
(34) Heany, P. J.; Davis, A. M. *Science* **1995**, *269*, 1562−1565.
(35) Suda, J.; Matsushita, M. *J. Phys. Soc. Jpn.* **1995**, *64*, 348−351.
(36) Suda, J.; Nakayama, T.; Nakahara, A.; Matsushita, M. *J. Phys. Soc. Jpn.* **1996**, *65*, 771−777.

(37) Suda, J.; Matsushita, M.; Izumi, K. *J. Phys. Soc. Jpn.* **2000**, *69*, 124−129.
(38) Punin, Yu. O.; Shtukenberg, A. G. *Autodeformation Defects in Crystals*; St. Petersburg University Press: St. Petersburg, Russia, 2008 (in Russian).
(39) Žorž, M. *Geologija* **1993**, *36*, 211−222.
(40) Shtukenberg, A. G.; Punin, Yu. O.; Kotelnikova, E. N. *Proc. Russ. Mineral. Soc.* **1993**, *122* (5), 53−63 (in Russian).
(41) Punin, Yu. O.; Artamonova, O. I. *Cryst. Rep.* **2001**, *46*, 138−143.
(42) Rinaudo, C.; Franchini-Angela, M.; Boistelle, R. *J. Cryst. Growth* **1988**, *89*, 257−266.
(43) Rinaudo, C.; Franchini-Angela, M. *Mineral. Mag.* **1989**, *53*, 479−482.
(44) Punin, Yu. O.; Boldyreva, O. M. *Physica Kristallizatsii*; Kalinin University Press: Kalinin, Russia, 1980; pp 46−55 (in Russian).
(45) Kuz'mina, M. A.; Moshkin, S. V.; Punin, Yu. O. *Physica Kristallizatsii*; Tver University Press: Tver, Russia, 1991; pp 24−35 (in Russian).
(46) Shtukenberg, A. G.; Freudenthal, J.; Kahr, B. *J. Am. Chem. Soc.* **2010**, *132*, 9341−9349.
(47) Calvert, P. D.; Uhlmann, D. R. *J. Polym. Sci., Polym. Phys. Ed.* **1973**, *11*, 457−465.
(48) Ho, D. M.; Pascal, R. A. Jr. *Chem. Mater.* **1993**, *5*, 1358−1361.
(49) Kawabata, K.; Kumagai, T.; Mizutani, M.; Sambong, T. *J. Phys. I* **1996**, *6*, 1575−1580.
(50) Wellems, T. E.; Josephs, R. *J. Mol. Biol.* **1980**, *137*, 443−450.
(51) Yu, L. *J. Am. Chem. Soc.* **2003**, *125*, 6380−6381.
(52) Tao, J.; Yu, L. *J. Phys. Chem. B* **2006**, *110*, 7098−7101.
(53) Gunn, E. Small Molecule Banded Spherulites. Ph.D. Dissertation, University of Washington, Seattle, Washington, 2009.
(54) Fronczek, F. R.; Kamelb, H. N.; Slattery, M. *Acta Crystallogr.* **2003**, *C59*, o567−o570.
(55) Ye, H.-M.; Xu, J.; Guo, B.-H.; Iwata, T. *Macromolecules* **2009**, *42*, 694−701.
(56) Maillard, D.; Prud'homme, R. E. *Macromolecules* **2008**, *41*, 1705−1712.
(57) Keith, H. D.; Padden, F. J. *J. Polym. Sci.* **1959**, *39*, 101−122.
(58) Keith, H. D.; Padden, F. J. *J. Polym. Sci.* **1959**, *39*, 123−138.
(59) Tao, J.; Jones, K. J.; Yu, L. *Cryst. Growth Des.* **2007**, *7*, 2410−2414.
(60) Jones, F. T.; Lee, K. S. *Microscope* **1970**, *18*, 279−285.
(61) Winchell, A. N. *The Optical Properties of Organic Compounds*; McCrone Research Institute: Chicago, 1987; p 113.
(62) Goldstein, D. H. *Polarized Light*, 2nd ed.; Marcel Dekker: New York, 2003.
(63) Takakura, Y.; Ahmad, J. E. *Appl. Opt.* **2007**, *46*, 7354−7364.
(64) Azzam, R. M. A. *Opt. Lett.* **1978**, *2*, 148−150.
(65) Goldstein, D. H. *Appl. Opt.* **1992**, *31*, 6676−6683.
(66) Hauge, P. S. *J. Opt. Soc. Am.* **1978**, *68*, 1519−1528.
(67) Schellman, J.; Jensen, H. P. *Chem. Rev.* **1987**, *87*, 1359−1399.
(68) Arteaga, O.; Canillas, A. *Opt. Lett.* **2010**, *35*, 559−561.
(69) Kaminsky, W.; Glazer, A. M. *Z. Kristallogr.* **1997**, *212*, 283−296.
(70) Sun, Y.; Zhu, L.; Kearns, K. L.; Ediger, M. D.; Yu, L. A. *Proc. Natl. Acad. Sci. U.S.A.* **2011**, *108*, 5990−5995.
(71) Bassett, D. C. *Philos. Trans. R. Soc. London, Ser. A* **1994**, *348*, 29−43.
(72) Bassett, D. C. *J. Macromol. Sci.* **2003**, *B42*, 227−256.
(73) Xu, J.; Guo, B.-H.; Zhang, Z.-M.; Zhou, J.-J.; Jiang, Y.; Yan, S.; Li, L.; Wu, Q.; Chen, G.-Q.; Schultz, J. M. *Macromolecules* **2004**, *37*, 4118−4123.
(74) Wang, T.; Wang, H.; Li, H.; Gan, Z.; Yan, S. *PhysChemPhys* **2009**, *11*, 1619−1627.
(75) Reusch, E. *Ann. Phys. Chem.* **1869**, *138*, 628−638.
(76) Joly, G.; Billard, J. *J. Opt. (Paris)* **1981**, *12*, 323−329.
(77) Ye, H.-M.; Xu, J.; Freudenthal, J.; Kahr, B. *J. Am. Chem. Soc.* **2011**, *133*, 13848−13851.
(78) Keller, A. *J. Polym. Sci.* **1955**, *17*, 291−308.
(79) Maillard, D.; Prud'homme, R. E. *Macromolecules* **2008**, *41*, 1705−1712.
(80) Xu, J.; Guo, B.-H.; Zhang, Z.-M.; Zhou, J.-J.; Jiang, Y.; Yan, S.; Li, L.; Wu, Q.; Chen, G.-Q.; Schultz, J. M. *Macromolecules* **2004**, *37*, 4118−4123.
(81) Shtukenberg, A. G.; Punin, Yu. O.; Gunn, E.; Kahr, B. *Chem. Rev.* **2012**, *112*, 1805−1838.
(82) Eshelby, J. D. *J. Appl. Phys.* **1953**, *24*, 176−179.
(83) Schultz, J. M.; Kinloch, D. R. *Polymer* **1969**, *10*, 271−278.
(84) Toda, A.; Arita, T.; Hikosaka, M.; Hobbs, J. K.; Miles, M. J. *J. Macromol. Sci.* **2003**, *B42*, 753−760.
(85) Bierman, M. J.; Lau, Y. K. A.; Kvit, A. V.; Schmitt, A. L.; Jin, S. *Science* **2008**, *320*, 1060−1063.
(86) Zhu, J.; Peng, H.; Marshall, A. F.; Barnett, D. M.; Nix, W. D.; Cui, Y. *Nat. Nanotechnol.* **2008**, *3*, 477−481.
(87) Schultz, J. M. *Polymer* **2003**, *44*, 433−411.
(88) Kahr, B.; Shtukenberg, A.; Gunn, E.; Carter, D. J.; Rohl, A. L. *Cryst. Growth Des.* **2011**, *11*, 2070−2073.
(89) Keith, H. D.; Padden, F. J. *Polymer* **1984**, *25*, 28−42.
(90) Keith, H. D.; Padden, F. J. *Macromolecules* **1996**, *29*, 7776−7786.
(91) Shtukenberg, A. G.; Punin, Yu. O. In *Optically Anomalous Crystals*; Kahr, B., Ed.; Springer: Dordrecht, The Netherlands, 2007.
(92) Tao, J.; Sun, Y.; Zhang, G. G. Z.; Yu, L. *Pharm. Res.* **2009**, *26*, 855−864.
(93) Imai, H.; Oaki, Y. *Angew. Chem., Int. Ed.* **2004**, *43*, 1363−1368.
(94) Timoshenko, S.; Goodier, J. N. *Theory of Elasticity*; McGraw-Hill: Singapore, 1982.
(95) Shuvalov, L. *Modern Crystallography*, Vol. *4*; Springer: Berlin, 2005.